AGU100 ADVANCING EARTH AND SPACE SCIENCE

Geophysical Research Letters

Key Points:
- Strength and peturbulence dissipation rate offshore is smaller than onshore, with a weak diurnal cycle
- Dissipation rate is larger when flow is from the land, usually in wintertime at this site
- Large wind veer is often associated with low turbulence at the site

Supporting Information:
- Supporting Information S1

Correspondence to:
N. Bodini,
nicola.bodini@colorado.edu

U.S. East Coast Lidar Measurements Show Offshore Wind Turbines Will Encounter Very Low Atmospheric Turbulence

Nicola Bodini[1] , Julie K. Lundquist[1,2] , and Anthony Kirincich[3]

[1]Department of Atmospheric and Oceanic Sciences, University of Colorado Boulder, Boulder, CO, USA, [2]National Renewable Energy Laboratory, Golden, CO, USA, [3]Woods Hole Oceanographic Institution, Woods Hole, MA, USA

Abstract The rapid growth of offshore wind energy requires accurate modeling of the wind resource, which can be depleted by wind farm wakes. Turbulence dissipation rate (ϵ) governs the accuracy of model predictions of hub-height wind speed and the development and erosion of wakes. Here we assess the variability of turbulence kinetic energy and ϵ using 13 months of observations from a profiling lidar deployed on a platform off the Massachusetts coast. Offshore, ϵ is 2 orders of magnitude smaller than onshore, with a subtle diurnal cycle. Wind direction influences the annual cycle of turbulence, with larger values in winter when the wind flows from the land, and smaller values in summer, when the wind flows from open ocean. Because of the weak turbulence, wind plant wakes will be stronger and persist farther downwind in summer.

1. Introduction

Wind energy continues to expand as one of the cleanest energy technologies, with its minimal operational carbon emissions (Boyle, 2004) and zero water consumption (Macknick et al., 2012). Because winds over the open ocean experience low levels of surface friction (Landberg, 2015), offshore winds tend to be stronger and steadier. Additionally, the cost of offshore wind energy is decreasing faster than expected (Stiesdal, 2016). Many favorable locations for offshore wind farm development are close to coastal areas with large electricity needs (Manwell et al., 2010), minimizing the need for long-distance transmission (Wiser et al., 2015).

Currently, most of the existing offshore wind farms are located in Northern Europe, where they account for a capacity of about 15GW, with a planned increase to about 74 GW by 2030 (van Hoof, 2017). In the United States, a single 30-MW commercial offshore wind farm (Deepwater Wind, 2016) has been built. However, the U.S. offshore technical resource potential is estimated to be nearly double the nation's current electricity use (Musial et al., 2016). Many offshore wind projects are currently being planned, mostly concentrated along the Eastern Seaboard. The state of Massachusetts plans to procure 1,600 MW of installed offshore wind, representing about 11% of its overall energy needs, by 2027 (Musial et al., 2017), with beneficial impacts on the state's economy and employment (Massachusetts Clean Energy Center et al., 2018).

As offshore wind energy development grows, accurate forecasting of the available wind resource in the offshore environment is required. Recent studies (Berg et al., 2019; Yang et al., 2017) show that the hub-height wind speed predicted by the Weather Research and Forecasting (WRF) model (Skamarock et al., 2005) is highly sensitive to the parametrization of turbulence dissipation rate (ϵ), which contributes up to 75% of the variance in hub-height wind speed. Therefore, improved representations of ϵ in models are crucially needed to enhance the accuracy of wind energy forecasting.

Turbulence also plays a key role in the development and subsequent erosion of wind turbine and wind farm wakes, whose spatial extent can be particularly long offshore (Platis et al., 2018; Siedersleben, Lundquist et al., 2018; Siedersleben, Platis, et al., 2018), with observed wakes extending beyond 45 km in some cases. While the erosion of wakes is related to ambient turbulent kinetic energy, the dissipation of turbulence within the wake, which represents the first step of wake erosion, is defined by the turbulence dissipation rate. Therefore, an accurate model representation of ϵ would allow for a better layout optimization of offshore wind farms, which would in turn reduce the large costs related to wind farm wakes (Nygaard, 2014)
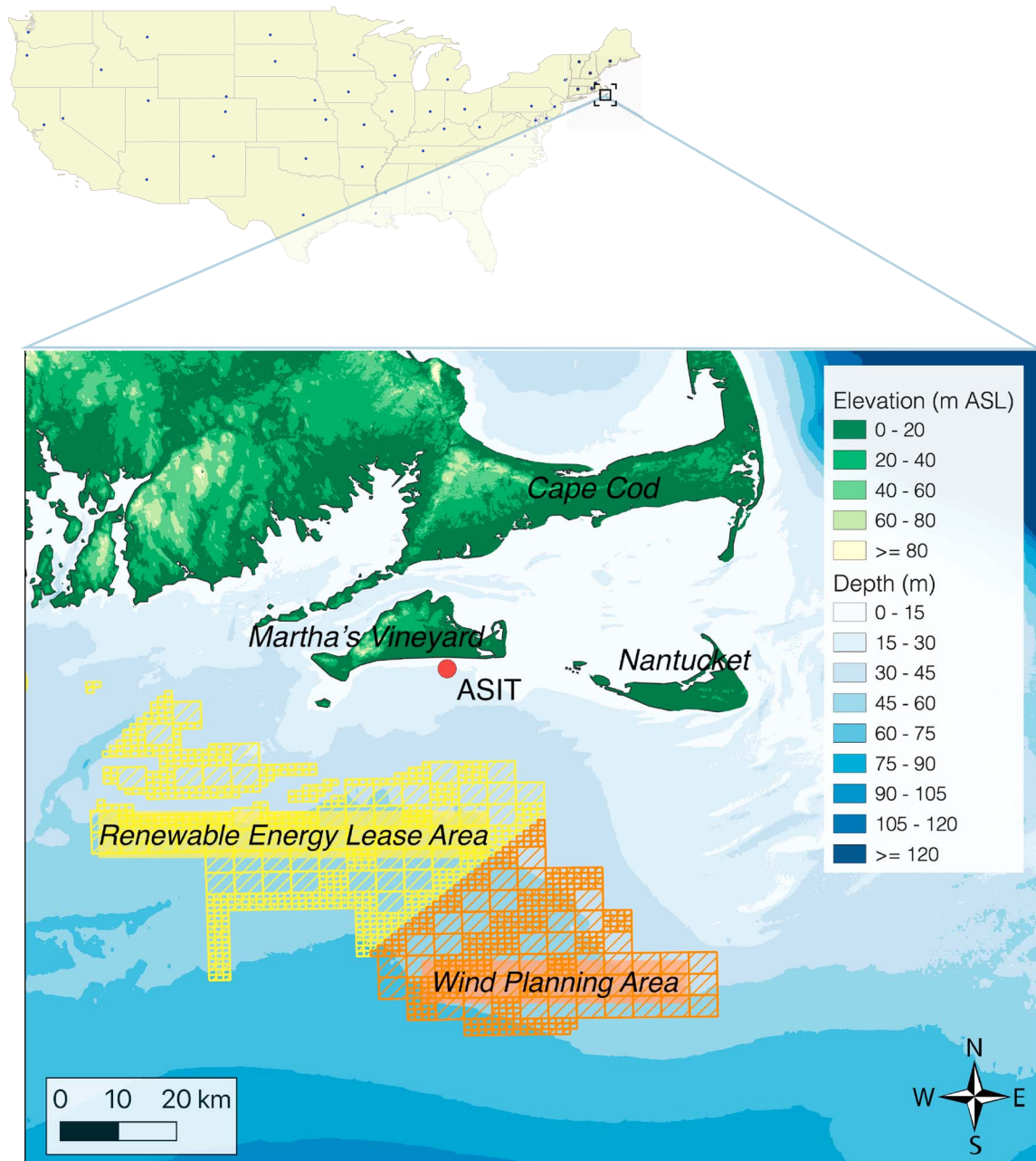
Figure 1. Map of the areas off the coasts of Rhode Island and Massachusetts where future development of offshore wind projects will take place. The location of the Air-Sea Interaction Tower (ASIT) platform, where the WINDCUBE v2 lidar used in this study was deployed, is shown. ASL = above mean sea level.

deriving from the uncoordinated development of wind projects (Lundquist et al., 2019). An assessment of the variability of ϵ from observations in the offshore atmospheric boundary layer is an essential first step toward reducing uncertainty in offshore wind energy forecasting and optimizing energy production.

Various techniques to retrieve turbulence dissipation rates from sonic anemometers (Champagne et al., 1977; Oncley et al., 1996), high-frequency hot-wire anemometers suspended on tethered lifting systems (Frehlich et al., 2006; Lundquist & Bariteau, 2015), or flown on aircrafts (Fairall et al., 1980) or unmanned aerial vehicles (Lawrence & Balsley, 2013) have been developed. Despite the potential drawback of their inherent volume averaging (Frehlich & Cornman, 2002; Wang et al., 2016), the ease of deployment and extended measurement range of remote sensing instruments have fueled research to derive methods to

retrieve ϵ from lidars (Banakh et al., 1996; Frehlich, 1994; O'Connor et al., 2010; Wulfmeyer et al., 2016) and radars (McCaffrey et al., 2017; Shaw & LeMone, 2003). The extension and application of these techniques have led to a systematic assessment of the variability of ϵ in both flat (Bodini et al., 2018) and complex terrain (Bodini et al., 2019). However, to the authors' knowledge, no comprehensive analysis of the variability of turbulence dissipation rate in the offshore environment has been completed.

Here, we assess the temporal variability of the turbulence dissipation rate retrieved from 13 months of observations from a wind-profiling lidar deployed on an offshore platform. In section 2 we describe the site and the method used to retrieve ϵ. Section 3 presents daily and seasonal variability of ϵ and its relation to wind direction and land influence. In section 4, we summarize and conclude our analysis.

2. Data and Methods

2.1. The Massachusetts MetOcean Initiative

A "MetOcean Initiative" (Filippelli et al., 2015) funded by the Massachusetts Clean Energy Center has collected continuous observations of the atmospheric boundary layer at the Woods Hole Oceanographic Institution's (WHOI) Air-Sea Interaction Tower (ASIT) since October 2016. The ASIT is a cabled, fixed platform located approximately 3 km south of Martha's Vineyard in 17 m of water (Figure 1), proximate to the Rhode Island and Massachusetts Wind Energy Areas, the United States' largest region under development for offshore wind energy extraction. At the site, a suite of wind resource monitoring equipment augmented the existing sensors deployed by WHOI's Martha's Vineyard Coastal Observatory, including a pair of cup anemometers above the top of the tower at 26 m above mean sea level (ASL), a wind vane at 23 m ASL, and a WINDUCUBE version (v2) profiling lidar on the main platform at 13 m ASL. All metocean data collected by WHOI for the project was validated by AWS Truepower. The v2 lidar measures line-of-sight velocity along the four cardinal directions with a nominal zenith angle of 28°, with an additional line-of-sight velocity measurement along the vertical. The lidar was positioned on a platform extending in the prevailing wind direction and rotated such that none of the measurement beams were affected by the tower structure. Each five-beam cycle was completed in approximately 5 s. The lidar took measurements at 10 heights: 53, 60, 80, 90, 100, 120, 140, 160, 180, and 200 m above sea level. Thus, the lidar-measured winds were above the level of, and not affected by, the tower structure, nor were they expected to exhibit any signal of wave motion. Data availability from the lidar was high, with relatively limited data loss with height (availability >95% at 53 m ASL, ~80% at 200 m ASL).

Here, we analyze the first 13 months of observations, from 7 October 2016 to 29 October 2017. Periods during which precipitation was recorded at WHOI's shore lab on the southern coast of Martha's Vineyard have been excluded from the analysis.

2.2. Turbulence Dissipation Rate from Profiling Lidars

Turbulence dissipation rate can be estimated from the variance of the line-of-sight velocity measured by profiling lidars following the approach proposed by O'Connor et al. (2010) and refined in Bodini et al. (2018), assuming locally homogeneous and isotropic turbulence. This approach derives ϵ by integrating the turbulence spectrum within the inertial subrange. To do so, the maximum length scale (and thus the sample size) to include in the calculation must be accurately chosen (Bodini et al., 2018; Tonttila et al., 2015). Here we use a local regression of the spectrum of the line-of-sight velocity to estimate the extension of the inertial subrange, as described and tested in Bodini et al. (2019). The distribution of sample size values is between 20 s (5th percentile) and 300 s (95th percentile). ϵ is then calculated as

$$\epsilon = 2\pi \left(\frac{2}{3a}\right)^{3/2} \left(\frac{\sigma_b^2}{L_N^{2/3} - L_1^{2/3}}\right)^{3/2}, \tag{1}$$

where $a = 0.52$ is the one-dimensional Kolmogorov constant (Paquin & Pond, 1971; Sreenivasan, 1995); $L_1 = Ut$, with U the horizontal wind speed and t the dwell time (i.e., the time the laser beam spends in a specific position to collect data); and $L_N = NL_1$, where N is the size of the line-of-sight velocity sample determined from the local regression of the experimental spectra. The variance σ_b^2 is calculated by subtracting a contribution due to the instrumental noise from the variance (averaged across the lidar beams) of
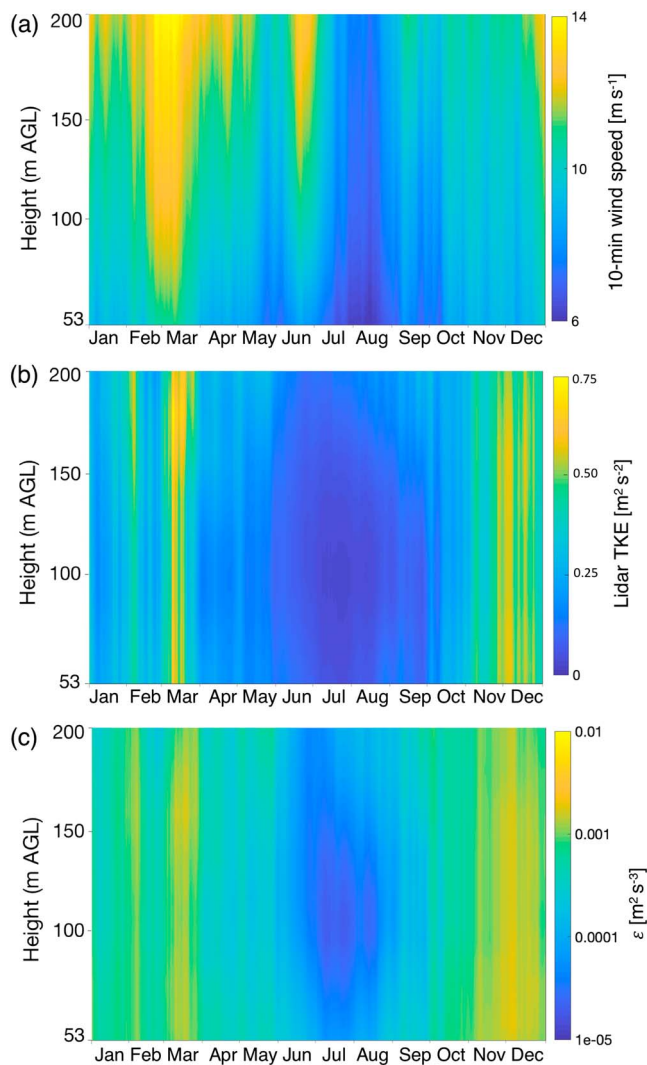
Figure 2. Annual cycle of (a) wind speed, (b) lidar turbulence kinetic energy (TKE), and (c) turbulence dissipation rate as measured by the Woods Hole Oceanographic Institution's Air-Sea Interaction Tower lidar. At each height, data have been smoothed using a 30-day running mean. Data from the overlapping calendar days in October 2016 and 2017 have been averaged.

line-of-sight velocity σ_v^2: $\sigma_b^2 = \sigma_v^2 - \sigma_e^2$, where σ_e^2 is defined as in equation (2) in Pearson et al. (2009; see the supporting information). More details of this method are available in Bodini et al. (2018, 2019).

3. Results

Turbulence dissipation occurs in an environment determined by wind speed, whose annual cycle at the site is shown in Figure 2a. Wind speeds are strong during winter, with average values above 10 m/s at wind-turbine hub-heights throughout the season, while summer shows smaller values, with minima in August, when the average wind speeds were less than 10 m/s at every observed height. Turbulence quantities also exhibit an annual cycle. We calculate turbulence kinetic energy (TKE) as

$$TKE = \frac{1}{2}\left(\sigma_u^2 + \sigma_v^2 + \sigma_w^2\right), \tag{2}$$

where the variances of the wind components are calculated over 2-min intervals. As noted by Sathe et al. (2011), lidars cannot fully resolve the wind variances, as a sonic anemometer would, given the lidars' limited temporal frequency. However, as data from a sonic anemometer are not available, we calculate TKE using lidar data and will refer to it as lidar TKE (Kumer et al., 2016; Rhodes & Lundquist, 2013). The annual cycle of lidar TKE (Figure 2b) reveals a clear pattern, with extremely small values during the summer, and larger values in winter, with little dependence on height. The annual variability of turbulence dissipation (Figure 2c) follows a similar pattern, with maximum in fall and winter, and summertime minima in the summer. Monthly average values of ϵ correlate well with monthly average lidar TKE ($R = 0.88$): When the kinetic energy of turbulence is large, large values of ϵ are usually needed to dissipate this energy. Monthly average wind speed has a smaller correlation with ϵ ($R = 0.71$), with some discrepancies (e.g., June). The annual cycle of ϵ at this offshore location contrasts from that in similar campaigns onshore, where the annual cycle of ϵ is mainly driven by the seasonal cycle of convection, with larger turbulence in summer due to increased convection, and more quiescent conditions in winter due to higher stratification (Bodini et al., 2019).

The annual variability of wind speed and turbulent properties impacts the average diurnal climatologies of these variables in different seasons (Figure 3). Wind speed tends to increase during the late afternoon and at night, while in daytime conditions lower average wind speeds occur, with weaker shear, as also found by Archer et al. (2016). On average, summer months (Figure 3b) show a larger diurnal cycle of wind speed compared to winter (Figure 3a). In contrast to this diurnal cycle in wind speed, the diurnal cycle of lidar TKE (Figures 3c and 3d) is subtle, with a small variability with height. The average diurnal cycles of ϵ offshore (Figures 3e and 3f) resemble that of lidar TKE, with differences greater than 1 order of magnitude between winter and summer. In summer, ϵ shows local minima at ~100 m ASL, and increased values at ~200 m ASL, especially during local morning. In contrast, in winter ϵ minima occur in the morning at ~200 m ASL. Average differences throughout the day in ϵ are smaller than 1 order of magnitude, whereas the diurnal cycle of ϵ onshore, in both flat (Bodini et al., 2018) and complex (Bodini et al., 2019) terrain, shows a larger amplitude, with differences of at least 1 order of magnitude between larger daytime values and smaller nighttime values. Moreover, average values of ϵ are smaller (in some cases by more than an order of magnitude) than onshore (Bodini et al., 2018, 2019).

The summer minimum in lidar TKE and turbulence dissipation rate occurs because of wind regimes. Northwesterly, westerly, and southwesterly winds dominate at the ASIT site (Figure 4a). Wind direction dictates
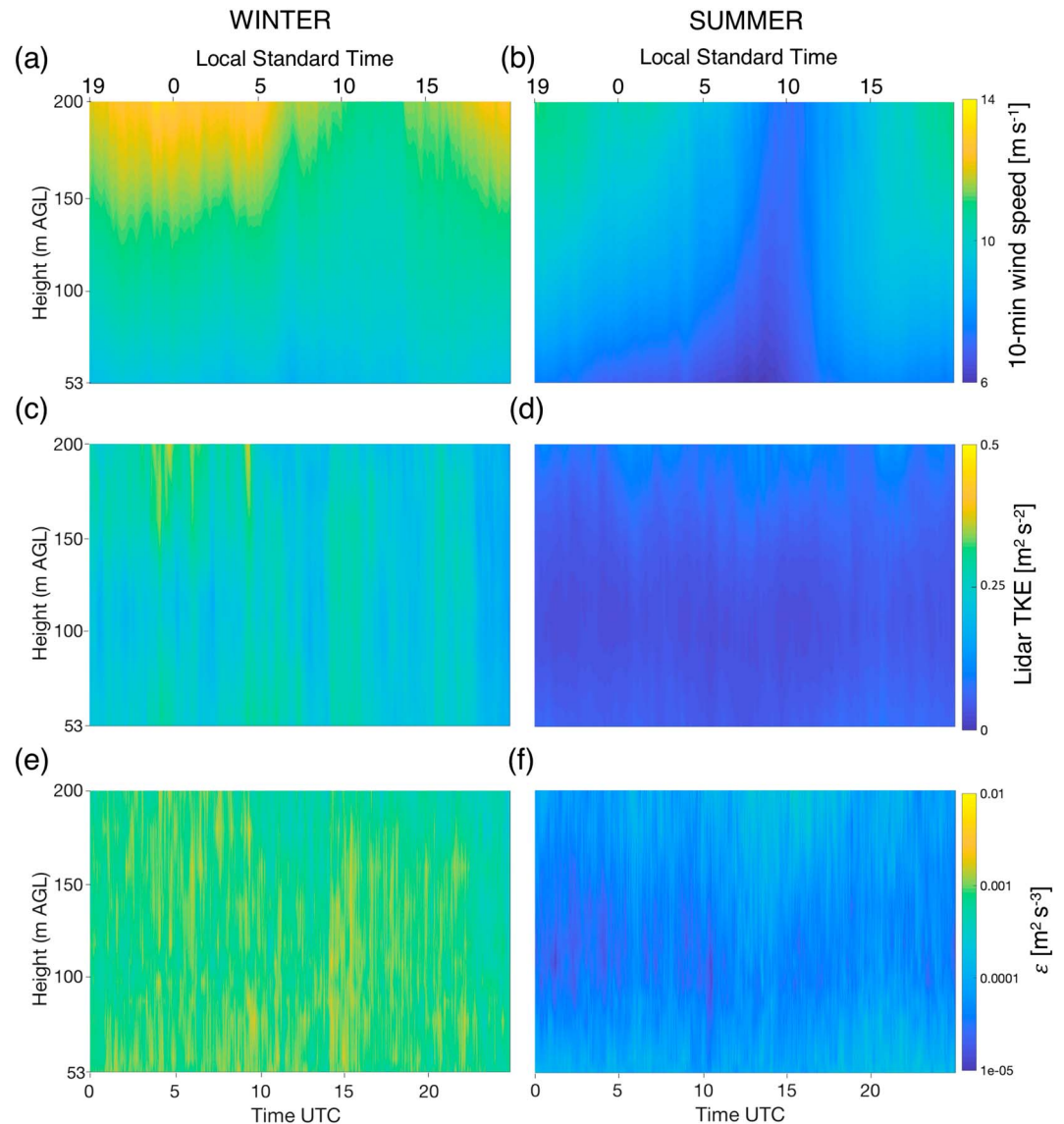
Figure 3. Average diurnal climatologies of wind speed, lidar turbulence kinetic energy (TKE), and turbulence dissipation rate for December, January, and February (panels a, c, and e) and June, July, and August (panels b, d, and f) as measured by the Woods Hole Oceanographic Institution's Air-Sea Interaction Tower lidar.

turbulence properties: Northwesterly winds generally lead to large values of lidar TKE and ϵ. In contrast, southwesterly winds generally cause low turbulence regimes (panels d and g). This relationship between wind direction and turbulence arises due to the location of the ASIT platform (Figure 1). During northwesterly winds, the flow interacts with the land before reaching the offshore platform. This land wake effect generates turbulence, both in terms of lidar TKE and ϵ. In contrast, southwesterly winds come from the open ocean, where lower roughness causes smaller values of lidar TKE and turbulence dissipation rates. In summer (June, July, and August), winds are almost exclusively southwesterly (Figure 4c), associated with lidar TKE generally smaller than 0.2 m²/s² (at 100 m ASL; Figure 4f) and turbulence dissipation rarely exceeding 10^{-3} m²/s³ (Figure 4i). In contrast, during winter, northwesterly winds dominate (Figure 4b), with larger TKE (Figure 4c) and ϵ (Figure 4h). The annual cycle of turbulence dissipation rate offshore is more influenced by the wind-land interaction rather than the seasonal cycle itself.

An annual cycle also emerges in wind veer, another important atmospheric variable that affects the structure of wind turbine wakes (Abkar et al., 2018; Bodini et al., 2017; Churchfield & Sirnivas, 2018). We calculate wind veer as the difference in 2-min average wind direction, calculated from the lidar, between 40 and 200
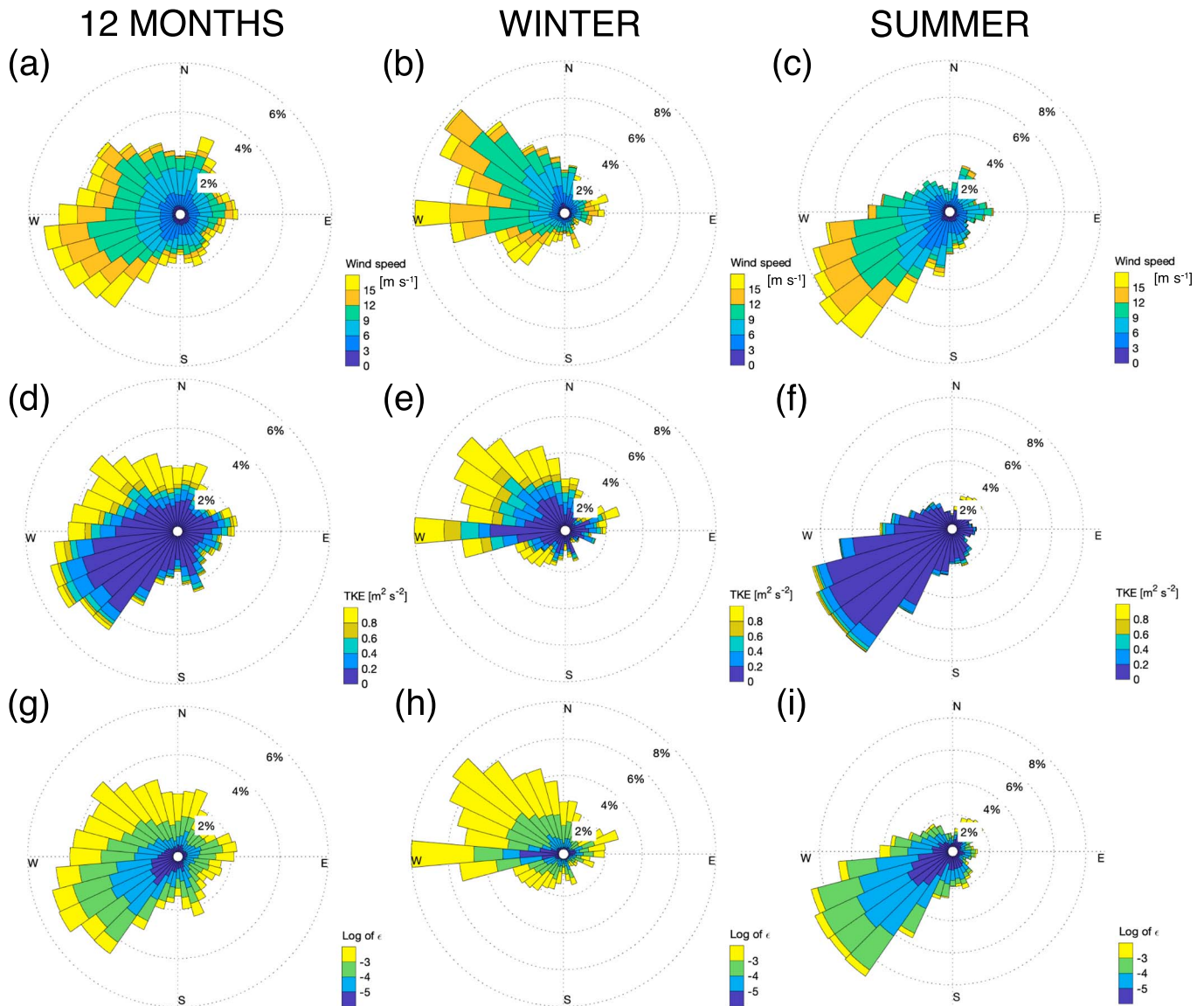
Figure 4. Roses of (a–c) wind speed, (d–f) lidar turbulence kinetic energy (TKE), and (g–i) turbulence dissipation rate, at 100 m, from the (a, d, and g) full 13-month period considered; (b, e, and h) December, January, and February; and (c, f, and i) June, July, and August, as measured by the Woods Hole Oceanographic Institution's Air-Sea Interaction Tower lidar.

m ASL, typical vertical limits for the rotor of offshore wind turbines. Wind veering occurs 70% of the time, with wind backing during 30% of the cases (histogram in the supporting information). Histograms of the absolute value wind veer and backing are shown in Figure 5. We highlight wind veer values with an average (between the chosen levels) wind speed between 3 and 13 m/s, corresponding to region 2, the area of the power curve where power is more sensitive to wind speed (Manwell et al., 2010), of the Siemens Gamesa 7.0 MW turbine. Large wind veer often occurs, with an average value of $0.07°$ m^{-1} ($0.08°$ m^{-1} for region 2 wind speeds) over the whole period of observations (panel a). However, important differences between the seasons emerge. In winter (panel b), the average wind veer wind ($0.05°$ m^{-1}, $0.04°$ m^{-1} for region 2 wind speeds) is only half of the summer average ($0.10°$ m^{-1}, $0.09°$ m^{-1} for region 2 wind speeds). The summertime offshore wind veer conditions are similar to the nighttime stable conditions found onshore in Walter et al. (2009). Veer is of particular interest with respect to wind turbine wake propagation (Bodini et al., 2017; Churchfield & Sirnivas, 2018) and wakes impact power production the most at wind speeds in region 2. The coupling of the strong veer in summertime with low dissipation will result in long-propagating but skewed wakes, impacting power production and turbulent loads on downwind turbines.
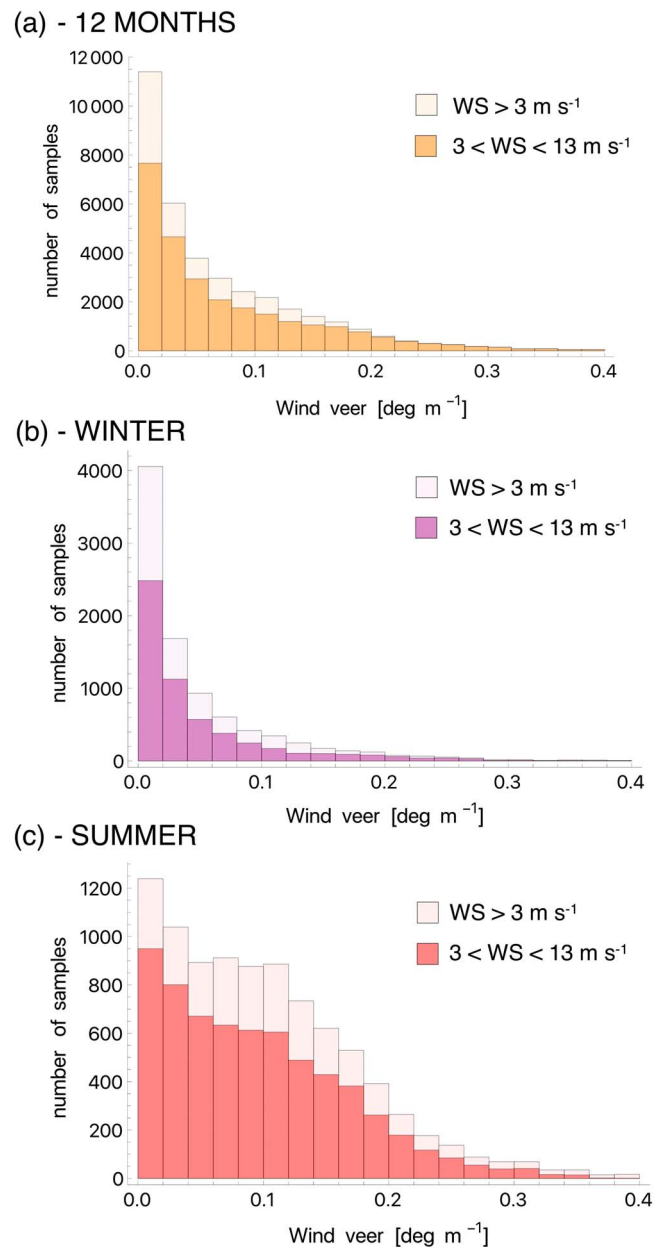
Figure 5. Histograms of 2-min average wind veer between 40 and 200 m above mean sea level as measured by the Woods Hole Oceanographic Institution's Air-Sea Interaction Tower lidar from the 13 months of observations (panel a); June, July, and August (panel b); and December, January, and February (panel c).

4. Discussion and Conclusions

Offshore wind power plant wakes can extend tens of km downwind (Platis et al., 2018; Siedersleben, Platis, et al., 2018; Siedersleben, Lundquist et al., 2018) in low-turbulence, stably stratified conditions. These wakes undermine offshore power production (Nygaard, 2014). Because wind power plant wake propagation is influenced by turbulence variability (Lundquist et al., 2019), we assess turbulence dissipation rate (ϵ) from a year-long data set of offshore wind lidar deployment.

We have retrieved ϵ from 13 months of observations from a profiling lidar located on an offshore platform ~3 km south of Martha's Vineyard. Offshore ϵ has, on average, smaller values compared to those found in comparable studies onshore, with a weak diurnal cycle. The small average values of ϵ are conducive to strong and long-lived wakes such as wakes observed in stable stratification in the North Sea (Platis et al., 2018;

Siedersleben, Lundquist et al., 2018; Siedersleben, Platis, et al., 2018). Moreover, this extended persistence of wakes will occur throughout the diurnal cycle, given the absence of strong turbulence dissipation even in convective daytime conditions. The seasonal cycle of ϵ is influenced by wind direction. When the wind comes from land, interactions between the wind and onshore topography increase TKE (and ϵ) observed offshore and, consequently, turbulence dissipation. Therefore, study of optimal layouts of offshore wind farms should consider the different turbulence regimes associated with the dominant wind patterns at each site, to take advantage of faster wake erosion connected to larger dissipation values caused by land wake effects.

Although offshore wind resource is considerable, and daily timing of wind speed increases from sea breezes are valuable for integrating wind energy into power grids, south-southwesterly flow would lead to increased wind speeds but also reduced turbulence, leading to more persistent wakes. Moreover, summertime wakes would be affected by wind veer greater than $0.3°$ m^{-1}; even larger values occur during wind gusts (Worsnop et al., 2017). This veer can impact effectiveness of wake steering solutions (Fleming et al., 2017, 2019) to minimize wake energy loss. Moreover, as wind farm lease areas are more than 25 km offshore, even the stronger turbulence conditions observed in the winter could represent an extreme upper bound on turbulence in the lease areas. The increased turbulence produced by the flow interaction with the land would likely dissipate further offshore. As offshore wind power plants in this region are developed, consideration of the likely persistence of wind power plant wakes will be required to predict the wind resource and effects of skewed wakes on turbine operations and maintenance costs.

Given the complexity of interactions between ϵ and other atmospheric variables, as well as the importance of the interaction with topography, machine learning techniques could improve the model parametrizations of ϵ, as already successfully done with other atmospheric phenomena (Gentine et al., 2018; Sharma et al., 2011; Xingjian et al., 2015).

References

Abkar, M., Sørensen, J., & Porté-Agel, F. (2018). An analytical model for the effect of vertical wind veer on wind turbine wakes. *Energies*, *11*(7), 1838.

Archer, C. L., Colle, B. A., Veron, D. L., Veron, F., & Sienkiewicz, M. J. (2016). On the predominance of unstable atmospheric conditions in the marine boundary layer offshore of the US northeastern coast. *Journal of Geophysical Research: Atmospheres*, *121*, 8869–8885. https://doi.org/10.1002/2016JD024896

Banakh, V., Werner, C., Köpp, F., & Smalikho, I. (1996). Measurement of the turbulent energy dissipation rate with a scanning doppler lidar. *Atmospheric and Oceanic Optics c/c of Optika Atmosfery I Okeana*, *9*, 849–853.

Berg, L. K., Liu, Y., Yang, B., Qian, Y., Olson, J., Pekour, M., et al. (2019). Sensitivity of turbine-height wind speeds to parameters in the planetary boundary-layer parametrization used in the Weather Research and Forecasting model: Extension to wintertime conditions. *Boundary-Layer Meteorology*, *170*, 507–518.

Bodini, N., Lundquist, J. K., Krishnamurthy, R., Pekour, M., Berg, L. K., & Choukulkar, A. (2019). Spatial and temporal variability of turbulence dissipation rate in complex terrain. *Atmospheric Chemistry and Physics*, *19*(7), 4367–4382.

Bodini, N., Lundquist, J. K., & Newsom, R. K. (2018). Estimation of turbulence dissipation rate and its variability from sonic anemometer and wind doppler lidar during the XPIA field campaign. *Atmospheric Measurement Techniques*, *11*(7), 4291–4308.

Bodini, N., Zardi, D., & Lundquist, J. K. (2017). Three-dimensional structure of wind turbine wakes as measured by scanning lidar. *Atmospheric Measurement Techniques*, *10*(8), 2881–2896.

Boyle, G. (2004). *Renewable energy*. Oxford, UK: Oxford University Press.

Champagne, F., Friehe, C., LaRue, J., & Wynagaard, J. (1977). Flux measurements, flux estimation techniques, and fine-scale turbulence measurements in the unstable surface layer over land. *Journal of the Atmospheric Sciences*, *34*(3), 515–530.

Churchfield, M. J., & Sirnivas, S. (2018). On the effects of wind turbine wake skew caused by wind veer. In *2018 wind energy symposium* (pp. 755). Kissimmee, FL.

Deepwater Wind (2016). Block island wind farm. Retrieved from http://dwwind.com/project/block-island-wind-farm

Fairall, C., Markson, R., Schacher, G., & Davidson, K. (1980). An aircraft study of turbulence dissipation rate and temperature structure function in the unstable marine atmospheric boundary layer. *Boundary-Layer Meteorology*, *19*(4), 453–469.

Filippelli, M. V., Markus, M., Eberhard, M., Bailey, B. H., & Dubois, L. (2015). Metocean data needs assessment and data collection strategy development for the Massachusetts wind energy area (Tech. Rep.) Retrieved from http://files.masscec.com/research/wind/MassCECMetoceanDataReport.pdf

Fleming, P., Annoni, J., Shah, J. J., Wang, L., Ananthan, S., Zhang, Z., et al. (2017). Field test of wake steering at an offshore wind farm. *Wind Energy Science*, *2*(1), 229–239.

Fleming, P., King, J., Dykes, K., Simley, E., Roadman, J., Scholbrock, A., et al. (2019). Initial results from a field campaign of wake steering applied at a commercial wind farm: Part 1. *Wind Energy Science Discussions, in review*, -. https://doi.org/10.5194/wes-2019-5

Frehlich, R. (1994). Coherent doppler lidar signal covariance including wind shear and wind turbulence. *Applied Optics*, *33*(27), 6472–6481.

Frehlich, R., & Cornman, L. (2002). Estimating spatial velocity statistics with coherent doppler lidar. *Journal of Atmospheric and Oceanic Technology*, *19*(3), 355–366.

Frehlich, R., Meillier, Y., Jensen, M. L., Balsley, B., & Sharman, R. (2006). Measurements of boundary layer profiles in an urban environment. *Journal of Applied Meteorology and Climatology*, *45*(6), 821–837.

Gentine, P., Pritchard, M., Rasp, S., Reinaudi, G., & Yacalis, G. (2018). Could machine learning break the convection parameterization deadlock? *Geophysical Research Letters*, *45*, 5742–5751. https://doi.org/10.1029/2018GL078202

Kumer, V.-M., Reuder, J., Dorninger, M., Zauner, R., & Grubišić, V. (2016). Turbulent kinetic energy estimates from profiling wind lidar measurements and their potential for wind energy applications. *Renewable Energy*, *99*, 898–910.

Landberg, L. (2015). *Meteorology for wind energy: An introduction*. Hoboken, NJ: John Wiley.

Lawrence, D. A., & Balsley, B. B. (2013). High-resolution atmospheric sensing of multiple atmospheric variables using the datahawk small airborne measurement system. *Journal of Atmospheric and Oceanic Technology*, *30*(10), 2352–2366.

Lundquist, J. K., & Bariteau, L (2015). Dissipation of turbulence in the wake of a wind turbine. *Boundary-Layer Meteorology*, *154*(2), 229–241.

Lundquist, J. K., DuVivier, K. K., Kaffine, D., & Tomaszewski, J. M. (2019). Costs and consequences of wind turbine wake effects arising from uncoordinated wind energy development. *Nature Energy*, *4*(1), 26–34.

Macknick, J., Newmark, R., Heath, G., & Hallett, K. C. (2012). Operational water consumption and withdrawal factors for electricity generating technologies: A review of existing literature. *Environmental Research Letters*, *7*(4), 45802.

Manwell, J. F., McGowan, J. G., & Rogers, A. L. (2010). *Wind energy explained: Theory, design and application*. Hoboken, NJ: John Wiley.

Massachusetts Clean Energy Center, Bristol Community College, UMass Dartmouth Public Policy Center, & Massachusetts Maritime Academy (2018). *2018 Massachusetts offshore wind workforce assessment*. Massachusetts Clean Energy Center.

McCaffrey, K., Bianco, L., & Wilczak, J. M. (2017). Improved observations of turbulence dissipation rates from wind profiling radars. *Atmospheric Measurement Techniques*, *10*(7), 2595–2611.

Musial, W., Beiter, P., Schwabe, P., Tian, T., Stehly, T., Spitsen, P., et al. (2017). 2016 offshore wind technologies market report (Tech. Rep.). Golden, CO: National Renewable Energy Laboratory (NREL). Retrieved from https://www.energy.gov/sites/prod/files/2017/08/f35/2016%20Offshore%20W%ind%20Technologies%20Market%20Report.pdf

Musial, W., Heimiller, D., Beiter, P., Scott, G., & Draxl, C. (2016). Offshore wind energy resource assessment for the United States (Tech. Rep.). Golden, CO: National Renewable Energy Laboratory (NREL). Retrieved from https://www.nrel.gov/docs/fy16osti/66599.pdf

Nygaard, N. G. (2014). Wakes in very large wind farms and the effect of neighbouring wind farms. *Journal of Physics: Conference Series*, *524*, 12162.

O'Connor, E. J., Illingworth, A. J., Brooks, I. M., Westbrook, C. D., Hogan, R. J., Davies, F., & Brooks, B. J. (2010). A method for estimating the turbulent kinetic energy dissipation rate from a vertically pointing doppler lidar, and independent evaluation from balloon-borne in situ measurements. *Journal of Atmospheric and Oceanic Technology*, *27*(10), 1652–1664.

Oncley, S. P., Friehe, C. A., Larue, J. C., Businger, J. A., Itsweire, E. C., & Chang, S. S. (1996). Surface-layer fluxes, profiles, and turbulence measurements over uniform terrain under near-neutral conditions. *Journal of the Atmospheric Sciences*, *53*(7), 1029–1044.

Paquin, J., & Pond, S. (1971). The determination of the kolmogoroff constants for velocity, temperature and humidity fluctuations from second-and third-order structure functions. *Journal of Fluid Mechanics*, *50*(2), 257–269.

Pearson, G., Davies, F., & Collier, C. (2009). An analysis of the performance of the UFAM pulsed doppler lidar for observing the boundary layer. *Journal of Atmospheric and Oceanic Technology*, *26*(2), 240–250.

Platis, A., Siedersleben, S. K., Bange, J., Lampert, A., Bärfuss, K., Hankers, R., et al. (2018). First in situ evidence of wakes in the far field behind offshore wind farms. *Scientific Reports*, *8*(1), 2163.

Rhodes, M. E., & Lundquist, J. K. (2013). The effect of wind-turbine wakes on summertime US Midwest atmospheric wind profiles as observed with ground-based Doppler lidar. *Boundary-Layer Meteorology*, *149*(1), 85–103.

Sathe, A., Mann, J., Gottschall, J., & Courtney, M. (2011). Can wind lidars measure turbulence? *Journal of Atmospheric and Oceanic Technology*, *28*(7), 853–868.

Sharma, N., Sharma, P., Irwin, D., & Shenoy, P. (2011). Predicting solar generation from weather forecasts using machine learning. In 2011 IEEE international conference on smart grid communications (pp. 528–533).Brussels, Belgium.

Shaw, W. J., & LeMone, M. A. (2003). Turbulence dissipation rate measured by 915 MHz wind profiling radars compared with in-situ tower and aircraft data. In *12th symposium on meteorological observations and instrumentation*. Long Beach, CA. Retrieved from https://ams.confex.com/ams/pdfpapers/58647.pdf

Siedersleben, S., Lundquist, J. K., Platis, A., Bange, J., Bärfuss, K., Lampert, A., et al. (2018). Micrometeorological impacts of offshore wind farms as seen in observations and simulations. *Environmental Research Letters*, *13*(12), 124012.

Siedersleben, S., Platis, A., Lundquist, J. K., Lampert, A., Bärfuss, K., Cañadillas, B., et al. (2018). Evaluation of a wind farm parametrization for mesoscale atmospheric flow models with aircraft measurements. *Meteorologische Zeitschrift*, *27*(5), 401–415.

Skamarock, W. C., Klemp, J. B., Dudhia, J., Gill, D. O., Barker, D. M., Wang, W., & Powers, J. G. (2005). A description of the advanced research WRF version 2 (Tech. Rep.). Boulder, CO: National Center For Atmospheric Research, Mesoscale and Microscale Meteorology Div.

Sreenivasan, K. R. (1995). On the universality of the Kolmogorov constant. *Physics of Fluids*, *7*(11), 2778–2784.

Stiesdal, H. (2016). Midt i en disruptionstid, Ingeniren. Retrieved from https://ing.dk/blog/midt-disruptionstid-190449

Tonttila, J, O'Connor, E., Hellsten, A, Hirsikko, A, O'Dowd, C, Järvinen, H, & Räisänen, P (2015). Turbulent structure and scaling of the inertial subrange in a stratocumulus-topped boundary layer observed by a doppler lidar. *Atmospheric Chemistry and Physics*, *15*(10), 5873–5885.

van Hoof, J. (2017). Unlocking Europe's offshore wind potential (Tech. Rep.). PricewaterhouseCoopers B.V. Retrieved from https://www.pwc.nl/nl/assets/documents/pwc-unlocking-europes-offshore-w%ind-potential.pdf

Walter, K., Weiss, C. C., Swift, A. H., Chapman, J., & Kelley, N. D. (2009). Speed and direction shear in the stable nocturnal boundary layer. *Journal of Solar Energy Engineering*, *131*(1), 11013.

Wang, H., Barthelmie, R. J., Pryor, S. C., & Brown, G. (2016). Lidar arc scan uncertainty reduction through scanning geometry optimization. *Atmospheric Measurement Techniques*, *9*(4), 1653–1669.

Wiser, R., Lantz, E., Mai, T., Zayas, J., DeMeo, E., Eugeni, E., et al. (2015). Wind vision: A new era for wind power in the United States. *The Electricity Journal*, *28*(9), 120–132.

Worsnop, R. P., Lundquist, J. K., Bryan, G. H., Damiani, R., & Musial, W. (2017). Gusts and shear within hurricane eyewalls can exceed offshore wind turbine design standards. *Geophysical Research Letters*, *44*, 6413–6420. https://doi.org/10.1002/2017GL073537

Wulfmeyer, V., Muppa, S. K., Behrendt, A., Hammann, E., Späth, F., Sorbjan, Z., et al. (2016). Determination of convective boundary layer entrainment fluxes, dissipation rates, and the molecular destruction of variances: Theoretical description and a strategy for its confirmation with a novel lidar system synergy. *Journal of the Atmospheric Sciences*, *73*(2), 667–692.

Xingjian, S., Chen, Z., Wang, H., Yeung, D.-Y., Wong, W.-K., & Woo, W.-C. (2015). Convolutional LSTM network: A machine learning approach for precipitation nowcasting. In *Advances in neural information processing systems* (pp. 802–810).

Yang, B., Qian, Y., Berg, L. K., Ma, P.-L., Wharton, S., Bulaevskaya, V., et al. (2017). Sensitivity of turbine-height wind speeds to parameters in planetary boundary-layer and surface-layer schemes in the weather research and forecasting model. *Boundary-Layer Meteorology*, *162*(1), 117–142.